# The Estimation of Temperature Distribution in Cylindrical Battery Cells under Unknown Cooling Conditions

Youngki Kim, *Student Member, IEEE* Shankar Mohan, *Student Member, IEEE*, Jason B. Siegel, Anna G. Stefanopoulou, *Fellow, IEEE*, and Yi Ding

***Abstract*—The estimation of temperature inside battery cells requires accurate information about the cooling conditions even when the temperature of the battery surface is measured. This paper presents a novel approach of estimating temperature distribution inside cylindrical batteries under unknown convective cooling conditions. A computationally efficient thermal model is first developed using a polynomial approximation of the temperature profile inside the battery cell. The Dual Extended Kalman Filter (DEKF) is then applied for the identification of the convection coefficient and the estimation of temperature inside the battery. In the proposed modeling approach, the thermal properties are represented by volume averaged lumped values with uniformly distributed heat generation. The model is parameterized and validated using experimental data from a 2.3 Ah 26650 Lithium-Iron-Phosphate (LFP) battery cell with a forced-air convective cooling during hybrid electric vehicle (HEV) drive cycles. Experimental results show that the proposed DEKF-based estimation method can provide an accurate prediction of core temperature under unknown cooling condition by measuring the cell current, voltage, and surface and ambient temperature. The accuracy is such that the scheme cam also be used for fault detection of a cooling system malfunction.**

***Index Terms*—Lithium ion batteries, Thermal model, Reduced order model, Dual Extended Kalman Filter, Parameter identification**

## I. INTRODUCTION

OVER the past years, energy storage systems utilizing lithium ion (Li-ion) batteries have become one of the most critical components for realizing efficient and clean transportation systems through electrification of vehicles, e.g., hybrid electric vehicles (HEVs), plug-in hybrid electric vehicles (PHEVs), and electric vehicles(EVs). Li-ion batteries have several advantages – no memory effect, wide range of operating temperature, and high energy and power density [1], [2]. However, the Li-ion battery performance, cycle life and capacity are adversely affected by sustained operation at extreme (above $45^oC$ and below freezing) temperatures [3]–[6], a recurring problem in automotive applications where batteries are exposed to temperature extremes with frequent high current discharge/charge rate that cause internal heating. Thus, being able to estimate/predict the temperature distribution across cells and packs is vital for formulating power management strategies that are mindful of the performance limitations of these versatile power/energy sources. In general, the performance of the cooling system can be degraded due to various reasons such as dust on fan blades, partial blockage in pipes, motor/pump ageing, and even a motor/pump failure. When such a degradation or failure occurs, it is not possible to reject the heat generated from the battery cell. In this condition, the lifespan of the battery exposed to the extreme temperatures will be considerably shortened. Therefore, it is important to identify the convective heat coefficient not only to accurately estimate the temperature distribution inside the battery but also for fault detection to ensure safe and reliable operation of the vehicle system.

This paper considers a novel method for estimating temperature distribution inside cylindrical batteries with simultaneous estimation of the convective cooling condition. To achieve this goal, a computationally efficient thermal model for a cylindrical cell is utilized to estimate simultaneously the convection coefficient and radial temperature distribution of the cell. Unlike existing reduced order modeling approaches in [7]–[10], and [11], a polynomial approximation to the solution of the heat transfer problem is used; this approach facilitates a systematic estimation of core, surface, volume-averaged temperatures, and volume-averaged temperature gradients. Dual Extended Kalman Filter (DEKF) is applied for the identification of the convection coefficient and the temperature distribution inside a cylindrical battery cell. The proposed estimation method provides the capability of detecting the malfunction of cooling system by monitoring the difference between the identified and off-line predetermined convection coefficient. This benefit indicates that a significant rise in temperature can be prevented by augmenting the proposed method with other existing battery management strategies for the safe and robust operation.

This paper is organized as follows: Section II presents the convective heat transfer problem for a cylindrical battery cell and the reduced order thermal model. Model reduction is performed using a polynomial approximation of the partial differential equation (PDE) system. The thermal properties of the battery are experimentally identified and sensitivity of parameters is analyzed in Section III. In Section IV, the temperature estimator applying a Dual Extended Kalman filter by using the proposed model for estimating the core

Y. Kim, J. B. Siegel, and A. Stefanopoulou are with the Department of Mechanical Engineering, University of Michigan, Ann Arbor, MI, 48109 USA. e-mail: (youngki@umich.edu, siegeljb@umich.edu, annastef@umich.edu).

S. Mohan is with the Department of Electrical Engineering, University of Michigan, Ann Arbor, MI, 48109 USA. e-mail: (elemsn@umich.edu).

Y. Ding is with U.S. Army Tank Automotive Research, Development, and Engineering Center (TARDEC), Warren, Michigan, 48397 USA. e-mail:(yi.ding8.civ@mail.mil).

# Report Documentation Page

*Form Approved*
*OMB No. 0704-0188*



| 1. REPORT DATE | 2. REPORT TYPE | 3. DATES COVERED |
|---|---|---|
| **06 MAR 2013** | **Journal Article** | **06-09-2012 to 02-03-2013** |

| 4. TITLE AND SUBTITLE | 5a. CONTRACT NUMBER |
|---|---|
| **The Estimation of Temperature Distribution in Cylindrical Battery Cells under Unknown Cooling Conditions** | **W56HZV-04-2-0001** |
| | 5b. GRANT NUMBER |
| | 5c. PROGRAM ELEMENT NUMBER |
| 6. AUTHOR(S) | 5d. PROJECT NUMBER |
| **Youngki Kim; Shankar Mohan; Jason Siegel; Anna Stefanopoulou; Yi Ding** | 5e. TASK NUMBER |
| | 5f. WORK UNIT NUMBER |
| 7. PERFORMING ORGANIZATION NAME(S) AND ADDRESS(ES) | 8. PERFORMING ORGANIZATION REPORT NUMBER |
| **UNIVERSITY OF MICHIGAN,4260 Plymouth Road,Ann Arbor,Mi,48109** | **; #23698** |
| 9. SPONSORING/MONITORING AGENCY NAME(S) AND ADDRESS(ES) | 10. SPONSOR/MONITOR'S ACRONYM(S) |
| **U.S. Army TARDEC, 6501 East Eleven Mile Rd, Warren, Mi, 48397-5000** | **TARDEC** |
| | 11. SPONSOR/MONITOR'S REPORT NUMBER(S) |
| | **#23698** |

12. DISTRIBUTION/AVAILABILITY STATEMENT

**Approved for public release; distribution unlimited**

13. SUPPLEMENTARY NOTES

**IEEE Transactions on Vehicles Journal**

14. ABSTRACT

**The estimation of temperature inside battery cells requires accurate information about the cooling conditions even when the temperature of the battery surface is measured. This paper presents a novel approach of estimating temperature distribution inside cylindrical batteries under unknown convective cooling conditions. A computationally efficient thermal model is first developed using a polynomial approximation of the temperature profile inside the battery cell. The Dual Extended Kalman Filter (DEKF) is then applied for the identification of the convection coefficient and the estimation of temperature inside the battery. In the proposed modeling approach, the thermal properties are represented by volume averaged lumped values with uniformly distributed heat generation. The model is parameterized and validated using experimental data from a 2.3 Ah 26650 Lithium-Iron-Phosphate (LFP) battery cell with a forced-air convective cooling during hybrid electric vehicle (HEV) drive cycles. Experimental results show that the proposed DEKFbased estimation method can provide an accurate prediction of core temperature under unknown cooling condition by measuring the cell current, voltage, and surface and ambient temperature. The accuracy is such that the scheme cam also be used for fault detection of a cooling system malfunction.**

15. SUBJECT TERMS

**Lithium ion batteries, Thermal model, Reduced order model, Dual Extended Kalman Filter, Parameter identification**

| 16. SECURITY CLASSIFICATION OF: | | | 17. LIMITATION OF ABSTRACT | 18. NUMBER OF PAGES | 19a. NAME OF RESPONSIBLE PERSON |
|---|---|---|---|---|---|
| a. REPORT<br>**unclassified** | b. ABSTRACT<br>**unclassified** | c. THIS PAGE<br>**unclassified** | **Public Release** | **10** | |

**Standard Form 298 (Rev. 8-98)**
Prescribed by ANSI Std Z39-18

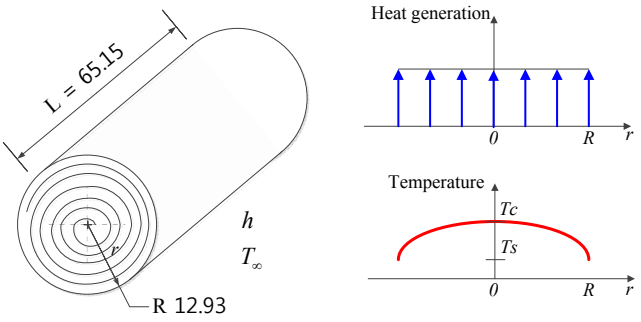


Fig. 1. Schematic for a A123 26650 cylindrical battery cell

temperature and identifying the convection coefficient. Section V presents and discusses experimental results and conclusions are drawn in Section VI.

## II. HEAT TRANSFER PROBLEM IN CYLINDRICAL BATTERIES

This paper considers the radially distributed (1-D) thermal behavior of a cylindrical battery cell with convective heat transfer boundary condition as illustrated in Fig. 1 [7], [12], [13]. A cylindrical Li-ion battery, so-called a jelly-roll, is fabricated by rolling a stack of cathode/separtor/anode layers. The individual layered sheets are thin, therefore, it is reasonable to assume uniform heat generation along the radial direction [13], [14]. Lumped parameters are used so that material properties such as thermal conductivity, density, and specific heat coefficient are assumed to be constant in a homogeneous and isotropic body. The thermal conductivity is one or two orders of magnitude higher in the axial direction than in the radial direction. Therefore, the temperature distribution in the axial direction will be more uniform [15], [16]. The governing equation of the 1-D temperature distribution $T(r,t)$ and boundary conditions are given by

$$\rho c_p \frac{\partial T(r,t)}{\partial t} = k_{th}\frac{\partial^2 T(r,t)}{\partial r^2} + \frac{k_{th}}{r}\frac{\partial T(r,t)}{\partial r} + \frac{Q(t)}{V_b}, \quad (1)$$

$$\text{B.C.'s } \left.\frac{\partial T(r,t)}{\partial r}\right|_{r=0} = 0, \quad (2)$$

$$\left.\frac{\partial T(r,t)}{\partial r}\right|_{r=R} = -\frac{h}{k_{th}}(T(R,t) - T_\infty), \quad (3)$$

where $t$, $\rho$, $c_p$ and $k_{th}$ represent time, volume-averaged density, specific heat coefficient, and thermal conductivity of the cell respectively. The radius of the battery cell is $R$, $Q$ is the heat generation inside the cell, and $V_b$ is the volume of battery cell. Ambient temperature for convection is denoted by $T_\infty$. The boundary condition in (2) represent the symmetric structure of the battery about the core. The other boundary condition shown in (3) represents the convective heat transfer at the surface of the battery.

### A. Model reduction

With evenly distributed heat generation, the temperature distribution along $r$-direction of the battery cell is assumed to satisfy the following polynomial approximation proposed in [17]

$$T(r,t) = a(t) + b(t)\left(\frac{r}{R}\right)^2 + d(t)\left(\frac{r}{R}\right)^4, \quad (4)$$

where $a(t)$, $b(t)$, and $d(t)$ are time-varying constants. To satisfy the symmetric boundary condition at the core of the battery cell, (4) contains only even powers of $r$. Thus, the temperatures at core and surface of the battery can be expressed as

$$T(0,t) = T_c = a(t), \quad (5)$$

$$T(R,t) = T_s = a(t) + b(t) + d(t), \quad (6)$$

where subscripts $c$ and $s$ denote core and surface respectively.

The volume-averaged temperature $\bar{T}$ and temperature gradient $\bar{\gamma}$ are introduced as follows:

$$\bar{T} = \frac{2}{R^2}\int_0^R rT\,dr, \quad (7)$$

$$\bar{\gamma} = \frac{2}{R^2}\int_0^R r\left(\frac{\partial T}{\partial r}\right)dr. \quad (8)$$

These volume-averaged values are used as the states unlike existing approaches in [8], [9], and [11].

By substituting (4) in (7) and (8), $\bar{T}$ and $\bar{\gamma}$ can be expressed in terms of constants as

$$\bar{T} = a(t) + \frac{b(t)}{2} + \frac{d(t)}{4}, \quad (9)$$

$$\bar{\gamma} = \frac{4b(t)}{3R} + \frac{8d(t)}{5R}. \quad (10)$$

By rearranging (6), (9), and (10), time-varying constants $a(t)$, $b(t)$, and $d(t)$ can be written by

$$a(t) = 4T_s - 3\bar{T} - \frac{15R}{8}\bar{\gamma}, \quad (11)$$

$$b(t) = -18T_s + 18\bar{T} + \frac{15R}{2}\bar{\gamma}, \quad (12)$$

$$d(t) = 15T_s - 15\bar{T} - \frac{45R}{8}\bar{\gamma}. \quad (13)$$

By substituting (11), (12), and (13) in (4), the temperature distribution can be expressed as a function of $T_s$, $\bar{T}$, and $\bar{\gamma}$

$$\begin{aligned} T(r,t) = {} & 4T_s - 3\bar{T} - \frac{15R}{8}\bar{\gamma} \\ & + \left[-18T_s + 18\bar{T} + \frac{15R}{2}\bar{\gamma}\right]\left(\frac{r}{R}\right)^2 \\ & + \left[15T_s - 15\bar{T} - \frac{45R}{8}\bar{\gamma}\right]\left(\frac{r}{R}\right)^4. \end{aligned} \quad (14)$$

The PDE (1) can be converted into ODEs by substituting (14) in volume-averaged governing equation and its partial derivative with respect to $r$ as follows:

$$\frac{d\bar{T}}{dt} + \frac{48\alpha}{R^2}\bar{T} - \frac{48\alpha}{R^2}T_s + \frac{15\alpha}{R}\bar{\gamma} - \frac{\alpha}{k_{th}V_b}Q = 0, \quad (15)$$

$$\frac{d\bar{\gamma}}{dt} + \frac{320\alpha}{R^3}\bar{T} - \frac{320\alpha}{R^3}T_s + \frac{120\alpha}{R^2}\bar{\gamma} = 0, \quad (16)$$

where $\alpha$ is thermal diffusivity and is defined as follows:

$$\alpha = k_{th}/\rho c_p. \quad (17)$$

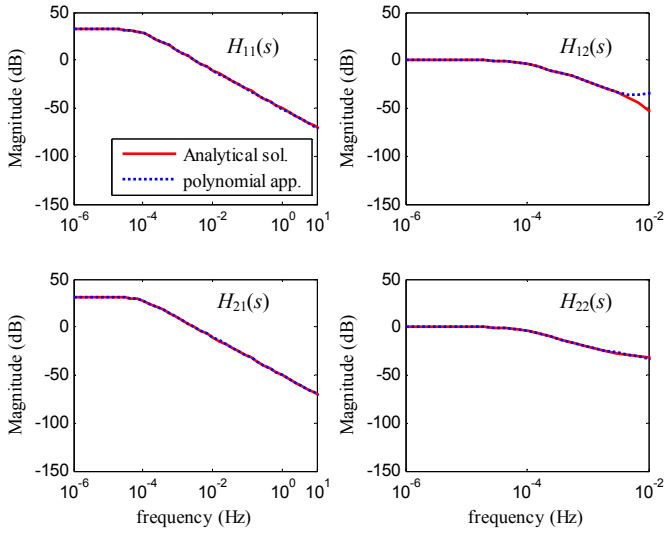


Fig. 2. Comparison of frequency response functions between analytical solution and polynomial approximation

Using (3), the surface temperature $T_s$ can be rewritten as

$$T_s = \frac{24k_{th}}{24k_{th}+Rh}\bar{T} + \frac{15k_{th}R}{48k_{th}+2Rh}\bar{\gamma} + \frac{Rh}{24k_{th}+Rh}T_\infty. \tag{18}$$

Finally, a two-state thermal model can be given by the following form:

$$\begin{aligned} \dot{x} &= Ax + Bu, \\ y &= Cx + Du, \end{aligned} \tag{19}$$

where $x = [\bar{T}\ \bar{\gamma}]^T$, $u = [Q\ T_\infty]^T$ and $y = [T_c\ T_s]^T$ are states, inputs and outputs respectively. System matrices $A$, $B$, $C$, and $D$ are defined as follows:

$$\begin{aligned} A &= \begin{bmatrix} \frac{-48\alpha h}{R(24k_{th}+Rh)} & \frac{-15\alpha h}{24k_{th}+Rh} \\ \frac{-320\alpha h}{R^2(24k_{th}+Rh)} & \frac{-120\alpha(4k_{th}+Rh)}{R^2(24k_{th}+Rh)} \end{bmatrix}, \\ B &= \begin{bmatrix} \frac{\alpha}{k_{th}V_b} & \frac{48\alpha h}{R(24k_{th}+Rh)} \\ 0 & \frac{320\alpha h}{R^2(24k_{th}+Rh)} \end{bmatrix}, \\ C &= \begin{bmatrix} \frac{24k_{th}-3Rh}{24k_{th}+Rh} & -\frac{120Rk_{th}+15R^2h}{8(24k_{th}+Rh)} \\ \frac{24k_{th}}{24k_{th}+Rh} & \frac{15Rk_{th}}{48k_{th}+2Rh} \end{bmatrix}, \\ D &= \begin{bmatrix} 0 & \frac{4Rh}{24k_{th}+Rh} \\ 0 & \frac{Rh}{24k_{th}+Rh} \end{bmatrix}. \end{aligned} \tag{20}$$

This state-space representation is used for the development of control design.

### B. Frequency domain analysis

The transfer function of the thermal system $H(s)$ is calculated by

$$H(s) = D + C(sI - A)^{-1}B, \tag{21}$$

where $s$ is Laplace variable.

The frequency response of transfer function of the proposed model is compared to that of the analytical solution in [7]. Parameters used to generate the plots in Fig. 2 are summarized in Table I. The heat transfer coefficient of $h$=5W/m$^2$K is chosen since this value is typical of natural convection condition [18].

TABLE I
PARAMETERS OF THE BATTERY [7]

| Parameter | Symbol | Value | Unit |
|---|---|---|---|
| Density | $\rho$ | 1824 | kg/m$^3$ |
| Specific heat coeff. | $c_p$ | 825 | J/kgK |
| Thermal conductivity | $k_{th}$ | 0.488 | W/mK |
| Convection coeff. | $h$ | 5 | W/m$^2$-K |
| Radius | $R$ | 12.93e-3 | m |
| Height | $L$ | 65.15e-3 | m |
| Volume | $V_b$ | 3.4219e-5 | m$^3$ |

Figure 2 shows that the effects of heat generation on core and surface temperature, denoted by $H_{11}(s)$ and $H_{21}(s)$ respectively, can be accurately predicted over the whole range of frequency. On the other hand, the responses of core and surface temperature excited by the ambient temperature, $H_{12}(s)$ and $H_{22}(s)$, are nearly identical to the analytical solution for frequencies below $10^{-2}$ Hz. In general, the temperature of cooling media does not change rapidly; thus, the prediction of temperature distribution using the proposed approach can be considered sufficiently accurate.

### C. Heat generation calculation

Since heat generation rate $Q$ is the input to the battery thermal system, the input needs to be accurately calculated from measurement data, such as current and voltage during operation. In [19], Bernardi et al. proposed the simplified form of heat generation rate with assumptions that heat generation due to enthalpy-of-mixing, phase-change, and heat capacity are assumed to be negligible expressed by

$$Q = i(U - V) - i\left(T\frac{\partial U}{\partial T}\right), \tag{22}$$

where $i$, $U$, and $V$ represent the current, the open-circuit voltage (OCV), and the terminal voltage respectively. As shown in Fig 3, the OCV is a function of the battery state-of-charge(SOC). This function is experimentally obtained by averaging the measured terminal voltages during charging and discharging a battery with C/20 current rate under a Constant Current Constant Voltage (CCCV) charging protocol.

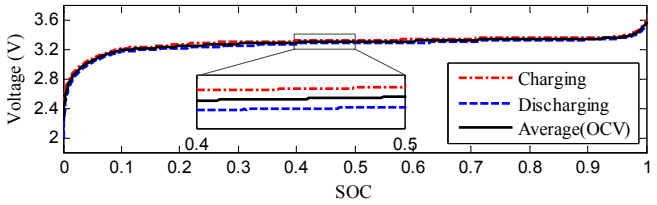


Fig. 3. Open-circuit voltage approximately obtained by averaging terminal voltages during charging and discharging a battery with C/20 current rate

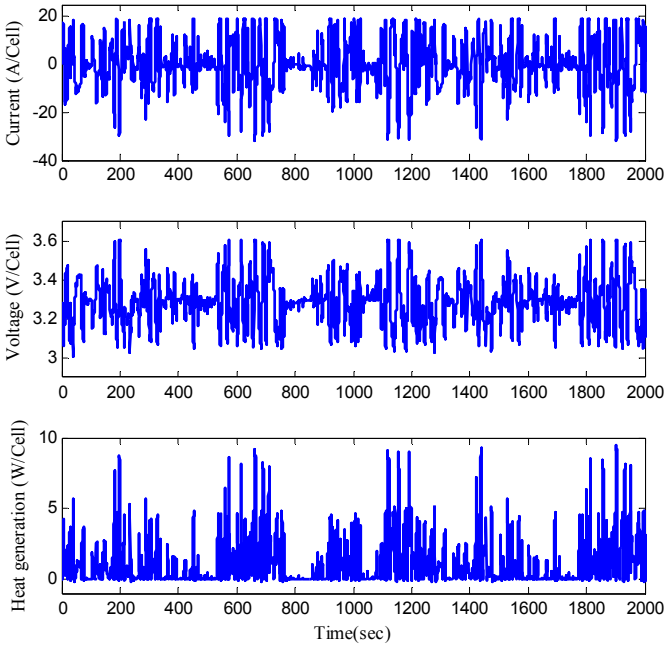


Fig. 4. Data set used for parameter ID: current (top), voltage (middle), and heat generation rate (bottom) during Urban-Assault Cycle

The OCV is then calculated at the estimated SOC value by integrating measured current with respect to time as

$$\frac{d\text{SOC}}{dt} = -\frac{I}{3600 Q_b} \tag{23}$$

where $Q_b$ is a battery capacity in Ah. The sign convention is such that positive current denotes battery discharging.

The last term in (22) is the heat generation from entropy change. In this paper, heat generation due to entropy change is neglected for simplicity. This simplification is warranted since the typical SOC range of HEV operation is between 40% and 60% in which $\frac{\partial U}{\partial T}$ of the battery cell is insignificant as shown in [9] for this chemistry. In addition, the reversible entropic heat generation would have zero mean value when the battery is operating in charge-sustaining mode, typical of HEV operation.

## III. PARAMETER IDENTIFICATION

In this section, the value of the lumped parameters in (19) for a 2.3 Ah 26650 LFP battery cell by A123 are identified through experimentation. Figure 4 shows current, voltage and calculated heat generation rate profiles over power demanding

TABLE II
IDENTIFIED THERMAL PROPERTIES

| Parameter | Symbol | Value | Reference |
|---|---|---|---|
| Density | $\rho$ | 2047* | 2118 [20] |
| Sp. heat coeff. | $c_p$ | 1148.1 | 1004.9–1102.6 [9], [21] |
| Thermal cond. | $k_{th}$ | 0.698 | 0.69 [20] |
| Conv. coeff. | $h$ | 60.00 | 65.99 [21] |

* Measured

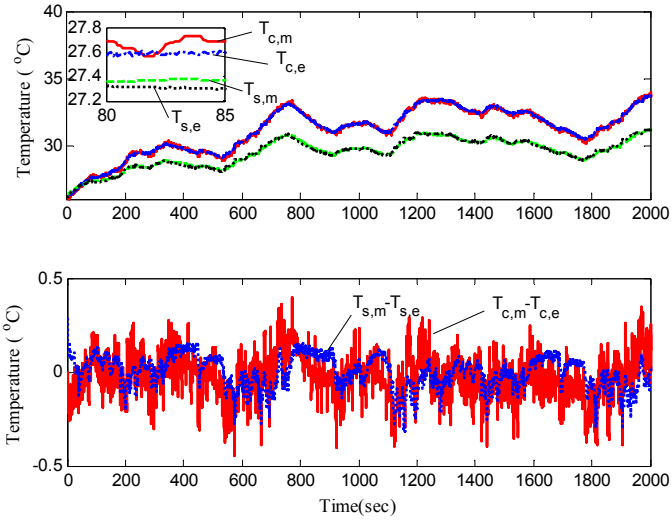


Fig. 5. Comparison between measured and simulated temperatures (top) and errors (bottom)

cycle used for military ground vehicle [22] Urban-Assault Cycle (UAC) that are used for the parametrization. The model is then validated using a different duty cycle. The numerical analysis on parameter sensitivity is performed to investigate the use of constant parameters for thermal conductivity and heat capacity and the importance of identifying the convection coefficient on-line.

### A. Identifying thermal properties

Parameter identification is important for accurately predicting the temperature distribution inside a battery cell as the parameters $k_{th}$, $c_p$, $\rho$, and $h$ determine the dynamics of thermal model. As the density can be assumed to be a measurable constant, only three parameters such as $k_{th}$, $c_p$, and $h$ are considered for the parameter identification. Following an experimental set-up in [21], we measured a cell current, voltage, surface and core temperature of the battery cell, and ambient temperature for parameter identification. As discussed in [21], some parameters are assumed to be known since all parameters are not identifiable without using the core temperature.

Let the error between the measured temperatures and model outputs at each time step $k$ in vector form be

$$e(k,\theta) = [T_{c,e}(k,\theta)\ \ T_{s,e}(k,\theta)]^T - [T_{c,m}(k)\ \ T_{s,m}(k)]^T, \tag{24}$$

where $\theta = [k_{th}\, c_p\, h]^T$, $T_{c,e}$ and $T_{s,e}$ represent the model parameters, core and surface temperatures respectively.

Parameters are identified by minimizing the Euclidean norm of the difference between the measured and simulated temperatures as given by

$$\theta^* = arg\min_{\theta} \sum_{k=1}^{N_f} ||e(k,\theta)||_2, \tag{25}$$

where $N_f$ is the number of measurement points. The minimization problem is solved by using the *fmincon* function in

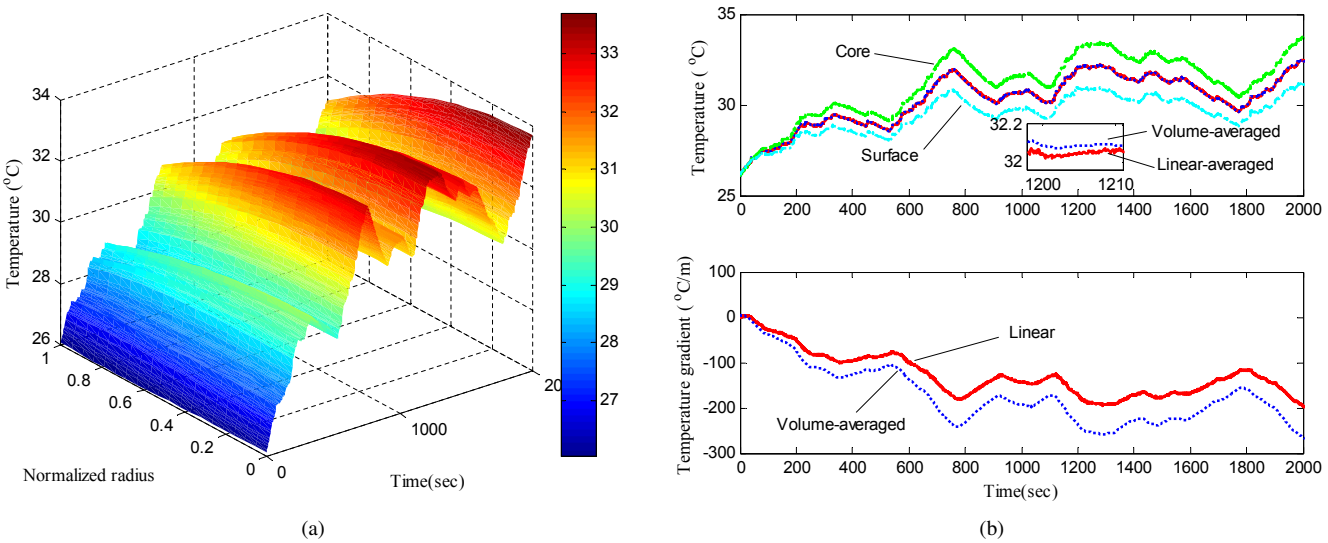


(a) (b)

Fig. 6. (a) Expected temperature distribution along the normalized radius ($r/R$) using polynomial approximation; (b) Cell temperature (top) and temperature gradient (bottom)

MATLAB; the parameters in Table I are used as initial guess for the identification.

Table II presents the identified thermal properties for the A123 26650 battery; these parameters are close to the values presented in the literature. The identified specific heat coefficient $c_p$ is 4% larger than the maximum value determined in [9] where $c_p$ was determined by measuring transient responses of the battery under different pulses. It was discussed that the deviation in identified value of $c_p$ might be caused by measurement uncertainty in temperature and the temperature dependency of the heat capacity.

Despite using similar experimental data and setup, the identified convection coefficient is 10% smaller than the coefficient calculated by using thermal resistance and battery surface area in [21]. This difference between our identified value and the one in [21] may be due to the two different model structures. Lin et al. in [21] considered two different materials, namely one for the core and one for the surface, whereas we assume the battery is a homogeneous and isotropic body. In order to accurately determine the convection coefficient, the temperature measurements of a pure metal during thermal relaxation can be used. For instance, the specific heat capacity of copper at 25$^o$C is known as 385 J/kgK. For more detailed description about the experiment, the interested reader is referred to [23].

Figure 5 shows the measured and simulated temperatures at the core and surface of the battery. The error between the measurements and simulated temperature is less than the sensor accuracy of 0.5$^o$C. Thermocouples used for temperature measurements are T-type whose accuracy is the maximum of 0.5$^o$C or 0.4% according to technical information from the manufacture, OMEGA. The parameterized thermal model accurately predicts the temperature inside the battery, which is difficult to measure in practical applications. Using (15), the temperature distribution inside the battery can be predicted as presented in Fig 6(a). Figure 6(b) shows the volume-averaged temperature and its gradient of the battery respectively. As evidenced in Fig. 6(b), there is no significant difference between the volume-averaged temperature and the linear average of core and surface temperatures, i.e. $(T_s + T_c)/2$. It should be noted that existing approaches in [8], [9], [11] have the capability of predicting the core temperature and have shown the efficacy of their proposed methods on the prediction of temperature inside the cell under consideration in this work. However, the phenomena may differ in the case of a cell with larger radius [24]. The volume-averaged temperature gradient is different from the linear temperature gradient, i.e. $(T_s - T_c)/R$; in particular, the volume-averaged temperature gradient is 1.36 times greater than linear temperature gradient under the UAC test. Since non-uniform temperature distribution can lead to accelerated capacity losses of inner core [24], the volume-averaged temperature gradient is an important metric to describe severity of temperature inhomogeneity inside the battery.

### B. Model validation

In order to validate the performance of the proposed model with identified parameters, the battery was tested under a different HEV drive cycle, the Escort Convoy Cycle (ECC). The current and voltage profiles for this cycle are illustrated in Fig 7(a). Figure 7(b) shows that there are slight differences between the measured and simulated temperatures; in particular, the root-mean-square errors (RMSE) of core and surface temperatures are 0.4 and 0.3$^o$C respectively. These differences may be explained with the assumption of radially uniform heat generation and high conductivity in the axial direction. Additionally, the hysteresis effect of the LFP battery is not properly considered in heat generation formulation (22), which might introduce error in the calculation of heat generation rate. Nevertheless, since the comparison of temperatures shows good agreement and reasonably small RMSEs, it can be concluded that the proposed model with identified thermal properties is sufficiently accurate for HEV drive cycles.

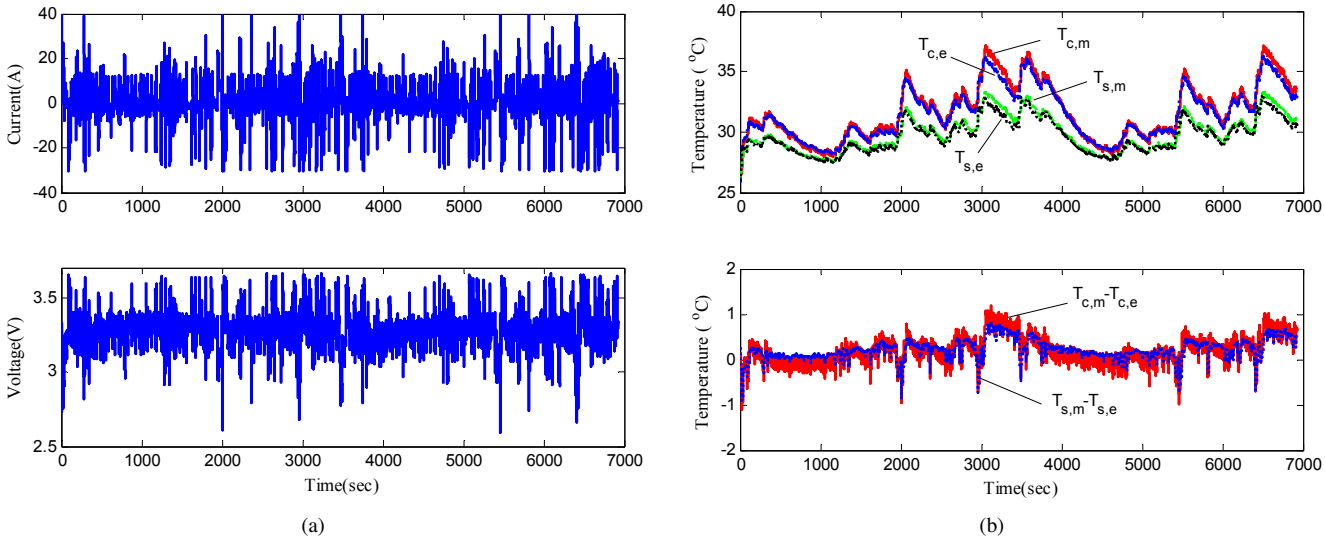


Fig. 7. (a) Current (top) and voltage (bottom) profiles during Escort Convoy cycle; (b) Validation data set: comparison between measured and simulated temperatures (top) and errors (bottom)

### C. Parameter sensitivity analysis

In order to investigate the impact of parameter variations on the performance of temperature prediction, each parameter is varied from the identified value while holding the other parameters constant. Figure 8 shows that parameters such as thermal conductivity $k_{th}$ and specific heat capacity $c_p$ have more influence on the prediction of core temperature than surface temperature. This result corresponds to the fact that the heat inside the battery cell is transferred through the conduction. On the other hand, the prediction of surface temperature is most sensitive to the variation of convection coefficient, which can be explained given the fact that the convection coefficient is directly related to the convective boundary condition (3). The convection coefficient has the most significant influence on the overall prediction of the core and surface temperature.

The specific heat coefficient and thermal conductivity are weakly dependent on temperature [9], [25], [26], so the assumption of constant parameters can be justified. On the other hand, the convection coefficient is highly dependent on fan speed or fluid velocity as expressed by empirical correlations provided by Zukauskas [27]. Consequently, the accurate identification of convection coefficient is important for better prediction of temperature inside the battery. This importance justifies the on-line identification of the convection coefficient for better estimation of temperature as detailed in Section IV.

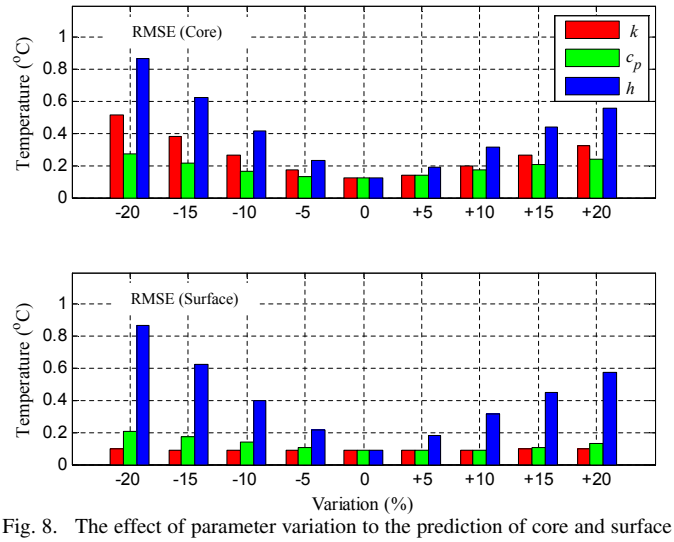


Fig. 8. The effect of parameter variation to the prediction of core and surface temperatures

## IV. ESTIMATION OF TEMPERATURE AND CONVECTION COEFFICIENT

As discussed in section III-C, the estimation of temperature inside the battery cell requires accurate knowledge of the convection coefficient which depends on cooling condition. In order to identify the convection coefficient on-line, the Dual Extended Kalman filter (DEKF) [28] is applied for better estimation of temperature distribution inside the battery cell. The other thermal parameters, such as thermal conductivity and specific heat coefficient, have less impact on temperature and do not change significantly over time. Therefore, the constant values identified in section III can be used.

Assuming the input $u(t)$ is constant over each sampling interval, a parameter varying (PV) discrete-time model at time step $k$ can be obtained as

$$\begin{aligned} x_{k+1} &= A_d(\theta_k)x_k + B_d(\theta_k)u_k, \\ y_k &= C(\theta_k)x_k + D(\theta_k)u_k, \end{aligned} \tag{26}$$

where $x = [\bar{T}\ \ \bar{\gamma}]^T$, $y = [T_c\ \ T_s]^T$, $\theta = h$, and $u = [Q\ \ T_\infty]^T$. System matrices $A_d \approx I + A\Delta T$ and $B_d = B\Delta T$ are obtained from matrices in (20) where the sampling period is $\Delta T$, and $I$ is the identity matrix.

Let the PV thermal system in discrete-time domain be

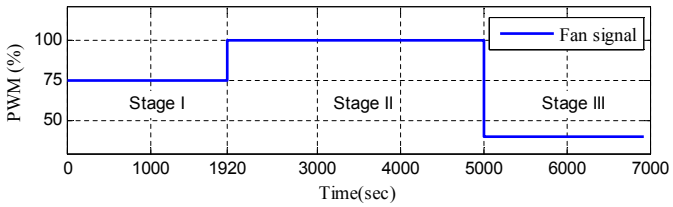


Fig. 9. Fan schedule for forced-air convective cooling

expressed in a general form by:

$$\begin{aligned} x_{k+1} &= f(x_k, u_k, \theta_k) + w_k, \\ y_k &= g(x_k, u_k, \theta_k) + v_k, \\ \theta_{k+1} &= \theta_k + r_k, \end{aligned} \tag{27}$$

where $w_k$, $v_k$, and $r_k$, are independent, zero-mean, Gaussian noise processes of covariance matrices $\Sigma_w$, $\Sigma_v$, and $\Sigma_r$, respectively. The design of the DEKF estimator is given as following update processes.

Time update for the parameter filter:

$$\hat{\theta}_k^- = \hat{\theta}_{k-1}^+, \tag{28}$$

$$S_k^- = S_{k-1}^+ + \Sigma_r. \tag{29}$$

Time update for the state filter:

$$\hat{x}_k^- = f(\hat{x}_{k-1}^+, u_{k-1}, \hat{\theta}_k^-), \tag{30}$$

$$P_k^- = A_{k-1} P_{k-1}^+ A_{k-1}^T + \Sigma_w. \tag{31}$$

Measurement update for the state filter:

$$K_k = P_k^- C_k^{x\,T} \left[ C_k^x P_k^- C_k^{x\,T} + \Sigma_v \right]^{-1}, \tag{32}$$

$$\hat{x}_k^+ = \hat{x}_k^- + K_k \left[ y_k - g(\hat{x}_k^-, u_k, \hat{\theta}_k^-) \right], \tag{33}$$

$$P_k^+ = \left[ I - K_k C_k^x \right] P_k^-. \tag{34}$$

Measurement update for the parameter filter:

$$L_k = S_k^- C_k^{\theta\,T} \left[ C_k^\theta P_k^- C_k^{\theta\,T} + \Sigma_e \right]^{-1}, \tag{35}$$

$$\hat{\theta}_k^+ = \hat{\theta}_k^- + L_k \left[ y_k - g(\hat{x}_k^-, u_k, \hat{\theta}_k^-) \right], \tag{36}$$

$$S_k^+ = \left[ I - L_k C_k^\theta \right] S_k^-, \tag{37}$$

where the matrices are calculated by

$$A_{k-1} = \frac{\partial f(x_{k-1}, u_{k-1}, \hat{\theta}_k^-)}{\partial x_{k-1}} \Big|_{x_{k-1}=\hat{x}_{k-1}^+} \tag{38}$$

$$C_k^x = \frac{\partial g(x_k, u_k, \hat{\theta}_k^-)}{\partial x_k} \Big|_{x_k=\hat{x}_k^-}, \tag{39}$$

$$C_k^\theta = \frac{dg(\hat{x}_k^-, u_k, \theta)}{d\theta} \Big|_{\theta=\hat{\theta}_k^-}. \tag{40}$$

The details of the matrices are provided in Appendix A. Superscripts $-$ and $+$ denote the *a priori* and *a posteriori* values respectively.

The identified states $\hat{x}$ and parameter $\hat{\theta}$, computed from the above DEKF algorithm, are used to estimate the core temperature in the battery cell from (26). The identified parameter can be also used for monitoring the malfunction or degradation

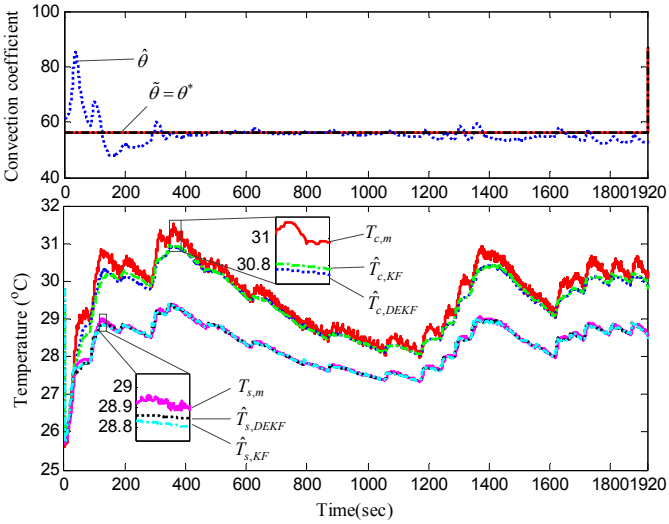


Fig. 10. Comparison of performance between KF estimator, DEKF estimator during stage I: convection coefficient (top) and temperature (bottom)

of cooling system. Under the assumption that the relationship between the convection coefficient and fan speed or PWM signal is known, the malfunction of the cooling system can be detected by comparing the identified parameter with a predetermined range of values $\theta^*$ based on the identification process performed at various cooling conditions. When the difference between the identified and predetermined values $|\hat{\theta} - \theta^*|$ is bounded and small, it can be considered that there is no fault in the cooling system. On the other hand, where $|\hat{\theta} - \theta^*| \gg \epsilon$ where $\epsilon$ is a pretuned threshold, a cooling fault can be detected. Furthermore, $|(\hat{\theta} - \theta^*)/\theta^*|$ can be interpreted as the severity of degradation of cooling system.

## V. EXPERIMENTAL RESULTS

In this section, the performance of the proposed temperature estimator using the DEKF is compared with that of the baseline Kalman Filter (KF) estimator without parameter identification. The battery is tested using the ECC under different cooling conditions. Three different forced convective cooling conditions (stage I, stage II, and stage III) are achieved by using different PWM signals driving the fan as shown in Fig. 9 which corresponds to an increase, followed by a decrease in the coolant flow rate. In order to investigate the influence of change in the parameter on the temperature estimation, the parameter is provided to each estimator as following:

- In stage I, the off-line predetermined convection coefficient is provided to the KF and is used for the DEKF as an initial value: $\tilde{\theta} = \theta^*$ and $\hat{\theta}(0) = \theta^*$
- In stage II, the off-line predetermined convection coefficient is provided to the KF only: $\tilde{\theta} = \theta^*$
- In stage III, two times larger convection coefficient compared to the known value is provided to the KF: $\tilde{\theta} = 2\theta^*$

where $\tilde{\theta}$ and $\hat{\theta}$ denote fixed and identified parameters for the KF and the DEKF respectively. Other thermal properties such as thermal conductivity and specific heat coefficient are assumed constant with values identified in section III.

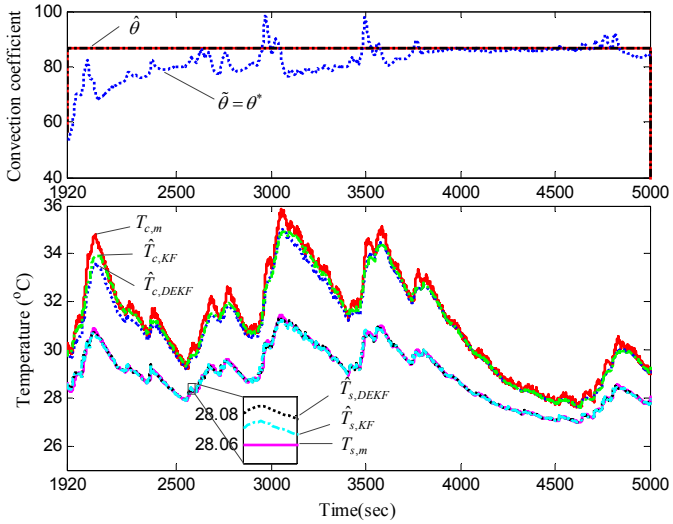


Fig. 11. Comparison of performance between KF estimator, DEKF estimator during stage II: convection coefficient (top) and temperature (bottom)

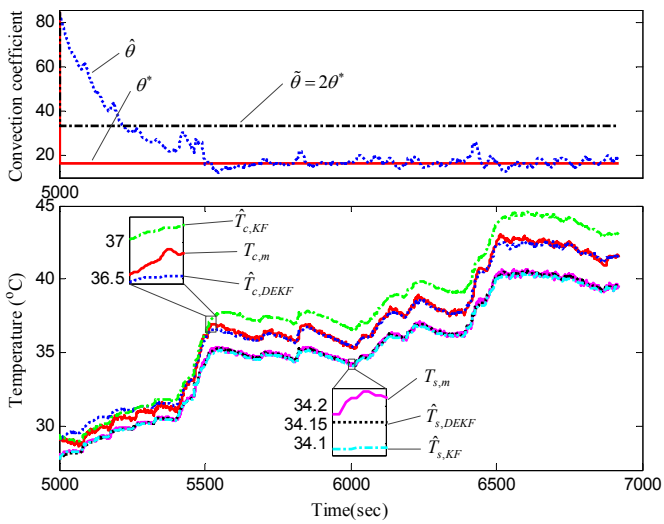


Fig. 12. Comparison of performance between KF estimator, DEKF estimator during stage III: convection coefficient (top) and temperature (bottom)

It is assumed that the initial temperature distribution inside the battery is uniform at 30$^o$C and convection coefficient is 56.2 $W/m^2K$, i.e. $\hat{x}(0) = [30\ 0]^T$ and $\hat{\theta}(0) = 56.2$ respectively. The covariance matrix for the state $\Sigma_w = {\beta_1}^2\text{diag}(1,1)$ describes the process noise where $\beta > 0$ is a parameter for tuning relaxed to model inaccuracy. The noise covariance $\Sigma_v = \sigma^2$ is determined from the standard deviation of temperature signal $\sigma = 0.05^o$C. The covariance matrix for the parameter $\Sigma_r = {\beta_2}^2$ influences the performance of noise filtering and the rate of parameter convergence. Ultimately, the initial condition of the error covariance matrix and the tuning parameter are chosen as $P(0) = \text{diag}(1,1)$, $\beta_1 = 0.0005$, $S(0) = 1$, and $\beta_2 = 0.01$ through repeated simulations respectively.

The results for the parameter and state estimation are shown in Fig. 10–12 and summarized in Table III. Figure 10 shows that the closed loop estimators can accurately predict temperature inside the battery. Even though the identified value is used as an initial guess for the parameter, it can be noticed that there is a large deviation in the initial part of the simulation. This deviation is caused by the error in the initial states. Nevertheless, the on-line identified parameter is close to the off-line determined value. Therefore, the performance of DEKF estimator is comparable to that of KF estimator. In particular, the RMSE for core temperature estimation by DEKF is 0.26, the same RMSE by the KF. Even though there is a slight error between the measured and estimated temperature, the closed loop estimators show a good performance in predicting core temperature overall. As discussed in Section III-C, thermal properties can vary with respect to operating temperature. Therefore, it is expected that better performance can be achieved by using temperature-dependent parameters for thermal conductivity and specific heat coefficient.

Figure 11 illustrates the performance of temperature estimation by the closed estimator in stage II when there are sudden changes in the cooling condition. The KF can accurately estimate the core temperature with information about the change in parameter value. Since the DEKF is capable of compensating inaccuracy in the parameter of the system, the DEKF provides reasonably accurate estimates for the core temperature by comparing the core temperature predicted by the KF estimator. Even though the RMSE for core temperature estimation by DEKF is slightly larger than the RMSE by the KF, the error is still reasonably small with considerations of the sensor accuracy.

As seen from Fig. 12, the KF estimator overestimates the core temperature when the incorrect parameter value is used as a convection coefficient. In other words, the reliable estimation of core temperature is only possible when the accurate parameter is available. Thus, it can be concluded that the DEKF estimator outperforms the KF estimator due to the capability of parameter identification. The RMSE for core temperature estimation in stage III can be substantially reduced from 1.18 to 0.31 by the DEKF. It is worthy to note that the DEKF can be augmented with other existing fault detection methods and power management strategies to improve the system robustness without cost increase. For instance, in order to detect partial blockage in cooling system, typically, a mass flow or pressure sensor is required. The DEKF enables the identification of convection coefficient by using sensors which are already equipped with the battery. Thus, by monitoring the difference between the identified and off-line predetermined values, the malfunction of cooling system can be detected.

TABLE III
PERFORMANCE OF TEMPERATURE ESTIMATION: RMSES FOR CORE AND SURFACE

| Method | DEKF | | KF | |
|---|---|---|---|---|
| Location | Core | Surface | Core | Surface |
| Stage I | 0.26 | 0.07 | 0.26 | 0.07 |
| Stage II | 0.39 | 0.08 | 0.29 | 0.08 |
| Stage III | 0.31 | 0.11 | 1.18 | 0.15 |

This performance tells that a significant rise in temperature can be prevented by limiting maximum discharge/charge current rate computed from the estimated parameter and states. Thus, the operation of the battery system can be safe and robust.

## VI. CONCLUSION

In this study, a method to estimate the temperature distribution in cylindrical batteries under unknown cooling condition is proposed. First, a radially distributed 1-D thermal modeling approach for a cylindrical battery cell is considered and polynomial approximation is applied to obtain a reduced order model enabling the development of real-time applications. Frequency domain analysis shows that the proposed model provides sufficiently accurate prediction of core and surface temperatures with a reasonable assumption that the temperature of cooling media does not change rapidly. The proposed model is used to identify thermal properties and convective coefficient for a 2.3 Ah 26650 LFP battery cell using a set of measured data. The numerical analysis on parameter sensitivity supports the use of constant parameters for thermal conductivity and heat capacity and the importance of identifying the convection coefficient on-line. Then, the Dual Extended Kalman Filter is applied to estimate the temperature inside the battery and convection coefficient by the cooling fan. The proposed method requires no knowledge of the convective cooling conditions. The results shows that the proposed DEKF estimator can provide reasonably accurate estimates of core temperature and convection coefficient by using surface temperature which is relatively easy to measure in practice. In addition, a faulty operation in the cooling system can be detected by monitoring the difference between the identified and off-line predetermined values. Since forced air is used as a cooling media to reject heat from the cell in this paper, the range of the convection coefficient of which we are interested is less than 100 W/m$^2$K. Therefore, the reader is urged to investigate whether the polynomial approximation is valid for their applications.

In the future, the proposed method can be used to develop various battery management strategies, e.g. the determination of maximum current with consideration of thermal constraints or optimal fan scheduling for energy efficiency, leading to the safe and efficient operation of the battery system.

## APPENDIX A

The matrices $A_{dk-1}$,$C_k^x$, and $C_k^\theta$ are calculated by

$$A_{dk-1} = \begin{bmatrix} 1 - \frac{48\alpha\hat{\theta}_k^-}{R(24k_{th}+R\hat{\theta}_k^-)} & \frac{-15\alpha\hat{\theta}_k^-}{24k_{th}+R\hat{\theta}_k^-} \\ \frac{-320\alpha\hat{\theta}_k^-}{R^2(24k_{th}+R\hat{\theta}_k^-)} & 1 - \frac{120\alpha(4k_{th}+R\hat{\theta}_k^-)}{R^2(24k_{th}+R\hat{\theta}_k^-)} \end{bmatrix},$$

$$C_k^x = \begin{bmatrix} \frac{24k_{th}-3R\hat{\theta}_k^-}{24k_{th}+R\hat{\theta}_k^-} & -\frac{120Rk_{th}+15R^2\hat{\theta}_k^-}{8(24k_{th}+R\hat{\theta}_k^-)} \\ \frac{24k_{th}}{24k_{th}+R\hat{\theta}_k^-} & \frac{15Rk_{th}}{48k_{th}+2R\hat{\theta}_k^-} \end{bmatrix},$$

$$C_k^\theta = \begin{bmatrix} \Psi_{11} & \Psi_{12} \end{bmatrix}\hat{x}_{k-1}^- + \begin{bmatrix} \Phi_{11} & \Phi_{12} \end{bmatrix}u_{k-1},$$

where

$$\Psi_{11} = -24k_{th}\frac{(24c_p\rho R^2k_{th}+3552\Delta Tk_{th}^2)+\hat{\theta}_k^-(c_p\rho R^3-148\Delta Tk_{th}R)}{c_p\rho R(24k_{th}+R\hat{\theta}_k^-)^3}$$

$$\Psi_{12} = -15k_{th}\frac{(24c_p\rho R^2k_{th}+3072\Delta Tk_{th}^2)+\hat{\theta}_k^-(c_p\rho R^3-168\Delta Tk_{th}R)}{2c_p\rho(24k_{th}+R\hat{\theta}_k^-)^3}$$

$$\Psi_{11} = -\frac{24R\Delta Tk_{th}}{V_bc_p\rho(24k_{th}+R\hat{\theta}_k^-)^2}$$

$$\Psi_{12} = 24k_{th}\frac{(24c_p\rho R^2k_{th}+3552\Delta Tk_{th}^2)+\hat{\theta}_k^-(c_p\rho R^3-148\Delta Tk_{th}R)}{Rc_p\rho(24k_{th}+R\hat{\theta}_k^-)^3}$$

## ACKNOWLEDGMENT

The authors wish to acknowledge the technical and financial support of the Automotive Research Center (ARC) in accordance with Cooperative Agreement W56HZV-04-2-0001 U.S. Army Tank Automotive Research, Development and Engineering Center (TARDEC) Warren, MI.

## REFERENCES

[1] R. Huggins, *Advanced Batteries: Materials Science Aspects, first edition*. Springer, 2008.

[2] W. S. Rao, Z., "A review of power battery thermal energy management," *Renewable and Sustainable Energy Reviews*, vol. 15, no. 9, pp. 4554–4571, 2011.

[3] J. Shim, R. Kostecki, T. Richardson, X. Song, and K. Striebel, "Electrochemical analysis for cycle performance and capacity fading of a lithium-ion battery cycled at elevated temperature," *Journal of Power Sources*, vol. 112, no. 1, pp. 222 – 230, 2002.

[4] X. Zhang, P. Ross, R. Kostecki, F. Kong, S. Sloop, J. Kerr, K. Striebel, E. Cairns, and F. McLarnon, "Diagnostic characterization of high power lithium-ion batteries for use in hybrid electric vehicles," *Journal of the Electrochemical Society*, vol. 148, no. 5, pp. 463–70, 2001.

[5] G. M. Ehrlich, "Lithium-ion batteries," in *Handbook of Batteries, third edition*. McGraw-Hill, 2002, ch. 35.

[6] S. Zhang, K. Xu, and T. Jow, "Low temperature performance of graphite electrode in li-ion cells," *Electrochimica Acta*, vol. 48, no. 3, pp. 241 – 246, 2002.

[7] M. Muratori, N. Ma, M. Canova, and Y. Guezennec, "A model order reduction method for the temperature estimation in a cylindrical li-ion battery cell," *ASME Dynamic Systems and Control Conference*, vol. 1, pp. 633–640, 2010.

[8] C. W. Park and A. K. Jaura, "Dynamic thermal model of li-ion battery for predictive behavior in hybrid and fuel cell vehicles," in *SAE World Congress 2003-01-2286*, 04 2003.

[9] C. Forgez, D. Vinh Do, G. Friedrich, M. Morcrette, and C. Delacourt, "Thermal modeling of a cylindrical lifepo4/graphite lithium-ion battery," *Journal of Power Sources*, vol. 195, no. 9, pp. 2961 – 2968, 2010.

[10] L. Cai and R. White, "An efficient electrochemical-thermal model for a lithium-ion cell by using the proper orthogonal decomposition method," *Journal of the Electrochemical Society*, vol. 157, no. 11, pp. A1188–A1195, 2010.

[11] X. Lin, A. G. Stefanopoulou, H. E. Perez, J. B. Siegel, Y. Li, and R. D. Anderson, "Quadruple adaptive observer of the core temperature in cylindrical li-ion batteries and their health monitoring," in *American Control Conference, June 27-29*, 2012.

[12] S. A. Hallaj, H. Maleki, J. Hong, and J. Selman, "Thermal modeling and design considerations of lithium-ion batteries," *Journal of Power Sources*, vol. 83, no. 1-2, pp. 1–8, 1999.

[13] D. R. Pendergast, E. P. DeMauro, M. Fletcher, E. Stimson, and J. C. Mollendorf, "A rechargeable lithium-ion battery module for underwater use," *Journal of Power Sources*, vol. 196, no. 2, pp. 793–800, 2011.

[14] D. H. Jeon and S. M. Baek, "Thermal modeling of cylindrical lithium ion battery during discharge cycle," *Energy Conversion and Management*, vol. 52, no. 8-9, pp. 2973–2981, 2011.

[15] H. Maleki, S. A. Hallaj, J. R. Selman, R. B. Dinwiddie, and H. Wang, "Thermal properties of lithium-ion battery and components," *Journal of The Electrochemical Society*, vol. 146, no. 3, pp. 947–954, 1999.

[16] S. Chen, C. Wan, and Y. Wang, "Thermal analysis of lithium-ion batteries," *Journal of Power Sources*, vol. 140, no. 1, pp. 111–124, 2005.

[17] V. R. Subramanian, V. D. Diwakar, and D. Tapriyal, "Efficient macro-micro scale coupled modeling of batteries," *Journal of the Electrochemical Society*, vol. 152, no. 10, pp. A2002 – A2008, 2005.

[18] J. Shi, F. Wu, S. Chen, and C. Zhang, "Thermal analysis of rapid charging nickel/metal hydride batteries," *Journal of Power Sources*, vol. 157, no. 1, pp. 592–599, 2006.
[19] D. Bernardi, E. Pawlikowski, and J. Newman, "General energy balance for battery systems." *Journal of the Electrochemical Society*, vol. 132, no. 1, pp. 5 – 12, 1985.
[20] H. Khasawneh, J. Neal, M. Canova, Y. Guezennec, R. Wayne, J. Taylor, M. Smalc, and J. Norley, "Analysis of heat-spreading thermal management solutions for lithium-ion batteries," *ASME Conference Proceedings*, vol. 2011, no. 54907, pp. 421–428, 2011.
[21] X. Lin, H. E. Perez, J. B. Siegel, A. G. Stefanopoulou, Y. Li, R. D. Anderson, Y. Ding, and M. P. Castanier, "Online parameterization of lumped thermal dynamics in cylindrical lithium ion batteries for core temperature estimation and health monitoring," *IEEE Transactions on Control System Technology, in press*, 2013.
[22] T.-K. Lee, Y. Kim, A. Stefanopoulou, and Z. Filipi, "Hybrid electric vehicle supervisory control design reflecting estimated lithium-ion battery electrochemical dynamics," 2011, pp. 388–395.
[23] K. Onda, H. Kameyama, T. Hanamoto, and K. Ito, "Experimental study on heat generation behavior of small lithium-ion secondary batteries," *Journal of the Electrochemical Society*, vol. 150, no. 3, pp. A285–A291, 2003.
[24] K. Smith, G.-H. Kim, and A. Pesaran, "Modeling of nonuniform degradation in large-format li-ion batteries," in *215th Electrochemical society meeting, May 25 - 29*, 2009.
[25] H. Maleki, J. Selman, R. Dinwiddie, and H. Wang, "High thermal conductivity negative electrode material for lithium-ion batteries," *Journal of Power Sources*, vol. 94, no. 1, pp. 26–35, 2001.
[26] K. Onda, T. Ohshima, M. Nakayama, K. Fukuda, and T. Araki, "Thermal behavior of small lithium-ion battery during rapid charge and discharge cycles," *Journal of Power Sources*, vol. 158, no. 1, pp. 535–542, 2006.
[27] A. Zukauskas, "Heat transfer from tubes in crossflow," ser. Advances in Heat Transfer, J. P. Hartnett and T. F. Irvine, Eds. Academic Press, 1972, vol. 8, pp. 93–160.
[28] E. A. Wan and A. T. Nelson, *Dual Extended Kalman Filter Methods*. John Wiley & Sons, Inc., 2002, pp. 123–173.

PLACE PHOTO HERE

**Youngki Kim** (S'13) is currently a Ph.D. Student in the Department of Mechanical Engineering at the University of Michigan, Ann Arbor, MI. He received his BS and MS degrees from the School of Mechanical and Aerospace Engineering at Seoul National University, Seoul, Republic of, Korea, in 2001 and 2003 respectively. He worked as a Research Engineer in the Research and Development Division at Hyundai Motor Company, Hwaseong, Republic of, Korea, from 2003 to 2008. His research interests include modeling and control of hybrid electric vehicles and lithium ion batteries.

PLACE PHOTO HERE

**Shankar Mohan**

PLACE PHOTO HERE

**Jason B. Siegel**

PLACE PHOTO HERE

**Anna G. Stefanopoulou** (F'09) is a Professor of mechanical engineering and the Director of the Automotive Research Center, University of Michigan, Ann Arbor. From 1998 to 2000, she was an Assistant Professor with the University of California, Santa Barbara. From 1996 to 1997, she was a Technical Specialist with Ford Motor Company. She has authored or co-authored more than 200 papers and a book. Her research interests are on estimation and control of internal combustion engines and electrochemical processes such as fuel cells and batteries. She holds 12 U.S. patents and is a Fellow of the ASME.

PLACE PHOTO HERE

**Yi Ding**